AMERICAN SCIENTIFIC PUBLISHERS
Copyright © 2026 by American Scientific Publishers
All rights reserved.
Printed in the United States of America

Journal of
Nanoelectronics and Optoelectronics
Vol. 21, pp. 126–139, 2026
www.aspbs.com/jno

ARTICLE

CMOS-Based Optimal Microgrid Structuring with Renewable Distributed Generators and Electric Vehicles

Kayalvizhi Saraswathi Balasubramanian[1,*] and Thenmalar Kaliannan[2]

The increasing penetration of renewable distributed generators (RDGs) and electric vehicles (EVs) introduces significant operational complexity in modern microgrids, demanding efficient optimization and low-power control architectures. This paper proposes a CMOS-based optimal microgrid structuring framework integrated with intelligent energy management for coordinated RDG and EV operation. A low-power CMOS control architecture is designed to enable real-time sensing, load forecasting, and bidirectional EV charging control while minimizing hardware energy consumption. The structural optimization of generation units, storage systems, and EV charging stations is achieved using the Waterwheel Plant Algorithm (WPA), which ensures enhanced convergence and global search capability. The proposed framework optimally determines generator placement, power dispatch scheduling, and EV charging strategies under varying load and renewable intermittency conditions. Simulation results demonstrate a reduction in total operational cost by 18.6%, power loss minimization by 21.3%, and voltage deviation improvement by 15.8% compared to conventional particle swarm and genetic algorithm-based approaches. The CMOS-based controller further reduces control power consumption by approximately 32% under sub-threshold operation. The integrated hardware–algorithm co-design approach enhances system reliability, scalability, and energy efficiency, making it suitable for next-generation smart microgrids with high EV penetration.

Keywords: CMOS-Based Energy Management, Microgrid Optimization, Renewable Distributed Generators, Electric Vehicles, Waterwheel Plant Algorithm, Low-Power Control Architecture, Smart Grid, Power Loss Minimization, Voltage Stability, Hardware–Algorithm Co-Design.

1. INTRODUCTION

1.1. Background

With ever-increasing customer demand in the distributed system (DS), the power system infrastructure must evolve. With rising interest in green technology, the use of Distributed Generation (DG) has improved significantly [1]. DGs are small-scale electricity production units, and their introduction into the DS has given numerous benefits. The incorporation of DGs has made the radial distribution system (RDS) more reliable due to greater grid efficiency, lower power losses, and a better voltage profile.

Various DG technologies are currently available on the market, with many still in the research and development stages [3]. These DG technologies are often classed based on their energization, which is either renewable or non-renewable [4]. Environmental benefits will make wind and solar-based DGs dominate the electricity market. As a result, renewable DGs (RDGs) now have a larger market share than their competitors [5]. However, the fundamental challenge with DG is their integration. There is a possibility that technical problems, including voltage quality and phase unbalance, will ensue if the integration of DG is not carried out appropriately [6].

Furthermore, due to the intermittent nature of wind and photovoltaic (PV), these DG types might cause a rise in power losses and voltage levels. Because most of our RDS suffers from high losses due to a high resistance to

[1]Department of Electrical and Electronics Engineering, Vivekanandha College of Engineering for Women (Autonomous), Elayampalayam, Tiruchengode, Namakkal 637205, Tamil Nadu, India
[2]Department of Electrical and Electronics Engineering, Vivekanandha College of Engineering for Women (Autonomous), Elayampalayam, Tiruchengode, Namakkal 637205, Tamil Nadu, India
*Author to whom correspondence should be addressed.
Email: sbkayalvizhi@gmail.com
Received: 5 April 2025
Accepted: 5 December 2025

reactance ratio, DG integration can assist make the system more dependable and efficient. However, the key to achieving this is to place the DGs in the best possible area. DGs that are optimally located in DS can reduce power loss, enhance voltage profile, and increase reliability. As a result, the right DG allocation in terms of placement and size into RDS is the primary responsibility for minimizing the aforementioned problems and reaping the benefits of DG integration [7].

1.2. Literature Review

Renewable-type DG installations in distribution network systems have increased because of environmental policies aimed at lowering carbon emissions. Furthermore, they are more cost-effective than standard DGs [8]. As a result, a considerable number of renewable-based DGs are beginning to take their position in the complicated DS. However, installing these DG units in less-than-optimal locations may result in greater system losses. Furthermore, when dealing with several DGs, optimum DG placement is critical to ensuring the entire system's stability and reliability [9]. In the event of several DG installations, the best location and sizing of DGs is typically handled using optimization [10–15]. Several authors have examined the question of optimal DG integration in the RDS from various perspectives. Therefore, to find the right allocation of DGs, the authors in [16] suggested an improved adaptive GA. For minimizing system costs, an effective framework has been developed in [17] to address the issue of optimal DG allocation. The authors of [18] then suggested integrating a GA with the Monte Carlo method to address the issue while factoring in the associated uncertainty. Following this, in [19], we learn about a method for optimally allocating resources to accommodate Plug-in Electric Vehicles (PEVs) and RDGs. Using the optimal scheduling in the RDS, the total cost reduction is accomplished in [20]. Furthermore, a cuckoo search algorithm (CSA) is employed on the integration of wind turbines (WTs) while taking uncertainties into consideration, using the scenario synthesis method. To assign ratings and positions to DGs, the authors later used Monte Carlo Simulation and the Crisscross Algorithm in [21]. Then, in [22], a new approach was suggested that used optimization capabilities of particle swarms.

The authors of [23] then developed a MILP-based probabilistic planning method and evaluated it in a rural RDS with the goals of optimizing integration and reducing line loss. For optimal RDG investment in distribution networks under uncertain scenarios, the authors create and assess a stochastic model in [24]. Reference [25] provided a framework for formulating a strategy for DG system planning that makes use of hydrogen energy storage and hybrid solar-wind power generation. Then, to find the optimal size and placement of DGs in an RDS while accounting for system uncertainties, a number of optimization algorithms were developed and evaluated, such as Grasshopper [28], Particle Swarm Optimization (PSO) [26], and modified sine cosine algorithm [27].

Furthermore, as demand grows, the necessity for dependable power system operation necessitates faster and more efficient algorithms to get the best value in a shorter amount of time. On that point, numerous unique intelligent and efficient algorithms, such as the Whale Optimization Algorithm (WOA) [29], Water Cycle Algorithm (WCA) Algorithm [30], Moth-Flame Optimization (MFO) Algorithm [31], and Artificial Bee Colony [32], are used for the optimization.

However, the majority of the preceding research do not take into account the RDGs' random nature. Taking unknown parameters into consideration will make the overall model more complex. However, such a model with a high processing weight produces a more accurate and efficient model. To deal with this, both input and network uncertainty must be addressed, with input uncertainties mostly caused by the dynamic behavior of load. To solve this issue, the authors of [33] provided an effective and robust model for the reconfiguration with load uncertainties. Furthermore, the authors of [34] used a probabilistic approach to investigate the renewable-based DGs. Later, to create a more robust model for distribution reconfiguration, the authors in [35] treated wind and photovoltaic power generation as double random and fuzzy uncertainty.

After that, [36] provided an approach using multiple scenarios for optimal RDS planning with RDGs and load demand uncertainties. The authors of [37] then developed a stochastic ranking algorithm to improve microgrid performance under demand unpredictability. A novel method was proposed in [38] to maximize RDG penetration in RDS. The authors also considered load unpredictability when reconfiguring. Next, [39] used the firefly algorithm to reconfigure RDS in an uncertain environment while accounting for DG seasonal power profiles. Later, [40] developed a backward reduction approach to minimize Monte-Carlo simulation possibilities to represent microgrid and RESs uncertainty. In [41], the authors focused mainly on technological challenges related to stability difficulties produced by high DG sources.

According to the above literature study, various works using intelligent algorithms have been tried and tested for the problem of network reconfiguration using non-renewable type DGs. Furthermore, there have been few studies on RDGs that take into account all of the uncertainties. Based on the above talks, a feasibility study on integrating RDGs into RDS can be conducted while taking into account the various economic restrictions. Furthermore, this allows us to create a complete MG planner and conduct cost and performance analyses. This work contributes the following.

(1) To solve RES based DGs and EV allocation issues in reconfigurable MGs, use VSI and WPA.

Downloaded by Scientific Tue, 10 Jun 2026 10:43:22
Copyright: American Scientific Publishers
Delivered by Ingenta

(2) The identification of weak and strong buses in each microgrid based on the voltage index determines DG and EV placement, respectively.
(3) Finding optimal microgrid configurations for distinct systems.
(4) EV specific constraints are properly identified and considered in the optimization problem. An effective electric vehicle charging and discharging system is suggested.

1.3. Paper Organization

The structure of this article is maintained below. The construction of the mathematical model, including the necessary objective functions and limits, is covered in Section 2. Section 3 explains the main research approach and the hybrid optimization strategies. Section 4 delves into a multitude of significant instances and outcomes. In Section 5, we present our study goal and summarize the obtained results.

2. PROBLEM FORMULATION

2.1. Objective Functions

An investigation of the parameters and characteristics of the items in MGs is carried out in order to find the best possible answer to the problem that has been presented. The mathematical functions are translated into the optimization problem through the process of studying the values of the parameters and attributes. Taking into consideration the information presented above, this article outlined three primary goals with the intention of reducing the overall economic cost of power transmission loss and the voltage deviation factor (VDF) of the bus. After that, these objective functions are maximized by means of the innovative intelligence algorithms while the system reconfiguration is being carried out.

2.1.1. Minimization of Power Transmission Loss

Internal sectionalizing switches can reconfigure the distribution system. Altering the switches' open/close status reveals the configurations and transmission losses for each. In each new configuration, the system's radial structure is tested for proper operation. The expression for the transmission loss (P_{tl}) of the system is given by,

$$P_{tl} = \sum_{i=1}^{nl} \sum_{j=1}^{np} I_{i,j}^2 * R_{i,j}$$

In the above equation, $I_{i,j}$ refers the i-th line j-th phase current which can be calculated through the load flow equations, and $R_{i,j}$ refers the i-th line j-th phase Resistance which can be obtained through the line characteristic data. The notations 'nl' and 'nb' refers total number of lines and buses connected to the system, respectively.

2.1.2. Minimization of OECC

This article examines two main MG power sources. First is the utility grid, then DGs. Under these circumstances, the entire cost of generation is determined by these two energy sources, which ought to be equivalent to the sum of the costs of generation from utility grids and generation from distributed generation systems.

$$TECC = TECC_{UG} + TECC_{PV} + TECC_{WT} \quad (1)$$

where $TECC$ is the total economic cost, $TECC_{UG}$, $TECC_{PV}$, $TECC_{WT}$ and $TECC_{FC}$ are the total economic cost of the utility grid, solar PV DGs, wind turbine DGs, and fuel cell DGs, respectively. Now, the individual expressions of all the above terms is considered from [40].

$$TECC_{UG} = \sum_{i=1}^{N_b} ECC_{UG} \quad (2)$$

where $ECC_{UG} = P_{UG} \times K_{UG}$. Here, P_{UG} and K_{UG} both stand for the electricity that comes from the utility and the coefficient that is utilized to determine the economic cost of the grid. All of the DG kinds' total economic cost expressions are derived from [40]. The PV economic cost expression is given as,

$$TECC_{PV} = \sum_{i=1}^{N_b} ECC_{PV,i} \quad (3)$$

where $ECC_{PV,i} = X_{PV} + Y_{PV} * PG_{PV}$. The expressions of X_{PV} and Y_{PV} are further given below.

$$X_{PV} = \frac{\text{Capital Cost_}PV * Psr * Ar}{\text{Lifetime_}PV * 8760 * LF} \quad (4)$$

$$Y_{PV} = \text{Cost_}PV_{O\&M} + \text{Cost_}PV_{\text{Fuel}}$$

In the above equation, the annual cost of PV installation is represented by X_{PV} and the overall cost for operation and maintenance is denoted by Y_{PV}. In similar manner, the economic cost of WT is expressed as:

$$TECC_{WT} = \sum_{i=1}^{N_b} ECC_{WT,i} \quad (5)$$

where $ECC_{WT,i} = X_{WT} + (Y_{Wt} * PV_{WT})$. The expressions of X_{WT} and Y_{WT} are further stated as:

$$X_{WT} = \frac{\text{Capital Cost_wind} * Pwr * Ar}{\text{Lifetime_wind} * 8760 * LF} \quad (6)$$

$$Y_{WT} = \text{Cost_}WT_{O\&M} + \text{Cost_}WT_{\text{Fuel}}$$

From the above equation, the annual cost of WT installation is represented by X_{WT} and the overall cost for operation and maintenance is denoted by $Y_{WT.}$ Moreover, the annual rate of benefit is denoted as Ar ($/hr) and the load factor of DGs are denoted by LF.

Figure 1 illustrates the overall architecture of the proposed CMOS-based optimal microgrid structuring framework. The upper layer represents the microgrid system comprising renewable generators (such as solar and wind),

Tue, 09 Jun 2026 10:13:52
Subject to ASP Terms of Use

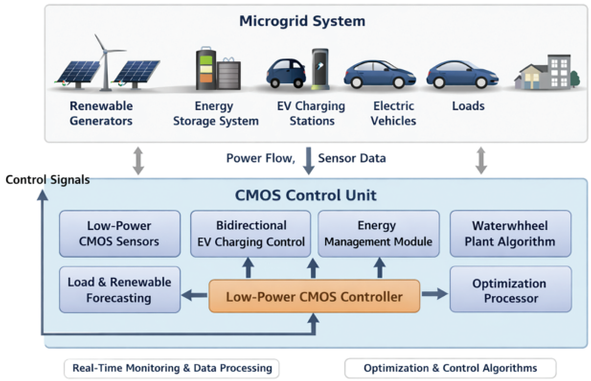


Fig. 1. CMOS-based control architecture for optimal microgrid structuring with renewable distributed generators and electric vehicles.

an energy storage system, EV charging stations, electric vehicles, and consumer loads. Bidirectional power flow and real-time sensor data are exchanged between the microgrid components and the control layer.

The lower layer presents the CMOS Control Unit, which forms the core intelligence of the system. It consists of low-power CMOS sensors for voltage, current, and state-of-charge monitoring, a load and renewable forecasting module, bidirectional EV charging control, and an energy management module. At the center, a low-power CMOS controller operates under sub-threshold conditions to minimize hardware energy consumption. The Waterwheel Plant Algorithm (WPA) is implemented within the optimization processor to determine optimal generator placement, power dispatch scheduling, and EV charging strategies.

This hardware–algorithm co-design enables real-time monitoring, reduced control power consumption, improved voltage stability, and minimized operational cost, making the system suitable for next-generation smart microgrids with high renewable and EV penetration.

2.1.3. Minimization of Bus VDF

The reliability of the electricity system depends on the voltage being constant. Maintaining a manageable bus voltage fluctuation factor is essential for enhancing the reliability of the distribution system. Subtracting the load bus voltage from the bus's real-time voltage yields the voltage deviation factor [4].

$$VDF = \sum_{i=1}^{N_{lb}} | V_i - V_{\mathrm{f}} | \tag{7}$$

V_i is the i-th bus voltage, V_{r} is the reference voltage, and N_{lb} denotes the number of load buses.

The figure presents the detailed circuit architecture of the proposed CMOS-based optimal microgrid system. Renewable energy sources such as solar PV and wind generators are interfaced to the common DC bus through controlled DC–DC converter stages (boost and buck converters). Each converter employs MOSFET switching devices driven by PWM signals generated from the low-power CMOS controller. The battery energy storage system is connected via a bidirectional buck–boost converter, enabling controlled charging and discharging based on load demand and renewable availability.

The EV charging station is integrated through a bidirectional converter supporting both grid-to-vehicle (G2V) and vehicle-to-grid (V2G) operation. Real-time voltage, current, and state-of-charge measurements are obtained using CMOS-based ADC sensing circuits. The centralized CMOS energy management unit executes the Waterwheel Plant Optimization Algorithm to determine optimal power dispatch, minimize losses, and regulate DC bus voltage. Operating under sub-threshold biasing conditions, the CMOS controller ensures reduced control power consumption while maintaining high dynamic response and system stability. This integrated circuit-level design enables efficient coordination between renewable generation, storage, and EV infrastructure in next-generation smart microgrids.

2.2. Constraints

The power system operational constraints are divided into two categories: equality constraints and inequality constraints. The classification of the constraints is based on the characteristics of the constraints.

IP: 103.252.4.234 On: Tue, 09 Jun 2026 10:13:52
Copyright: American Scientific Publishers
Delivered by Ingenta

2.2.1. Equality Constraint

The equality constraint is the distribution system power balancing equation. The total power input should equal all loads and transmission loss. These are the equations that describe the power balance:

$$\begin{cases} P_{UG} + \sum_{i=1}^{N_{\mathrm{DG}}} \mathrm{P}_{DG_i} = P_l + P_{ld} \\ Q_{UG} + \sum_{i=1}^{N_{\mathrm{DG}}} Q_{DG_i} = Q_l + Q_{ld} \end{cases} \tag{8}$$

P_{UG} and Q_{UG} denotes the real and reactive powers of utility grid, P_{DG_i} and Q_{DG_i} denotes the real and reactive powers of the i-th DG, P_l and Q_l represents the real and reactive power transmission losses, P_{ld} and Q_{ld} are the real active and reactive connected loads.

2.2.2. Inequality Constraints

Most of the time, they are conditional constraints that take into account system edges. On inequality constraints in power generation, [36] can be summarized as follows.

$$\max\left(P_i^{\min}, P_i^0 - DR_i\right) \le P_i \le \min\left(P_i^{\max}, P_i^0 + UR_i\right) \tag{9}$$

$$P_i \in \begin{cases} P_i^{\min} \le P_i \le P_{i,1}^l \\ P_{i,j-1}^u \le P_i \le P_{i,j}^l \\ P_{i,n_i}^u \le P_i \le P_i^{\max} \end{cases} \tag{10}$$

where current and previous output power are denoted by P_i and P_i^0. UR_i and DR_i are up-ramp and down-ramp limits of generating unit. The constraints of line flows are further considered from [4], [36]:

$$P_{G_i}^{\min} \le P_{G_i} \le P_{G_i}^{\max} \quad 1 \le i \le N_G \tag{11}$$

$$Q_{G_i}^{\min} \le Q_{G_i} \le Q_{G_i}^{\max} \quad 1 \le i \le N_G \tag{12}$$

$$Q_{C_i}^{\min} \le Q_{C_i} \le Q_{C_i}^{\max} \quad 1 \le i \le N_C \tag{13}$$

$$T_k^{\min} \le T_k \le T_k^{\max} \quad 1 \le k \le N_T \tag{14}$$

$$V_i^{\min} \le V_i \le V_i^{\max} \quad 1 \le i \le N_B \tag{15}$$

$$|S_k| \le S_k^{\max} \quad 1 \le k \le N_E \tag{16}$$

$$0.95 \le V_i \le 1.05, \quad i = 1, 2, \ldots, N_b \tag{17}$$

$$0.8 \le PF \le 1 \tag{18}$$

Due to current and voltage control loops, dispatchable DGs of various types of limit power handling capability. This affects real and reactive power $P_{\mathrm{DG},i,s}$ and $Q_{\mathrm{DG},i,s}$ generated by the DG follow the droop relationship [37]:

$$P_{\mathrm{DG},i,s} \le P_{DG,\,i,max}, \quad \forall i \in N_{\mathrm{droop}} \tag{19}$$

$$Q_{\mathrm{DG},i,s} \le Q_{\mathrm{DG},\,i,max}, \quad \forall i \in N_{\mathrm{droop}} \tag{20}$$

IP: 152.67.255.67 On: Tue, 09 Jun 2026 10:13:52
Copyright: American Scientific Publishers
Delivered by Ingenta

Due to the constraint limitations, the droop-controlled DG can be further modeled using the complementary constraints from [37] which is given by,

$$0 \le P_{\mathrm{DG}\,,\,i,\max} - P_{DG,\,i,s} \perp \frac{1}{m_{p,i}} \left(\omega_i^* - \omega_s\right) - P_{\mathrm{DG},\,i,s} \ge 0 \quad \forall i \in N_{\mathrm{droop}} \tag{21}$$

$$0 \le Q_{\mathrm{DG}\,,i,\max} - Q_{\mathrm{DG},\,i,s} \perp \frac{1}{n_{p,i}} \left(|V_k|^* - |V_{k,s}|\right) Q_{\mathrm{DG},i,s} \ge 0 \quad \forall i \in N_{\mathrm{droop}} \tag{22}$$

$$\sqrt{\left(P_{\mathrm{DG},i,s}\right)^2 + \left(Q_{\mathrm{DG},i,s}\right)^2} \le S_{\mathrm{DG},i,\max}, \quad \forall i \in N_{\mathrm{droop}} \tag{23}$$

Droop constraints [37]: The droop parameters in the dispatchable DG must be pre-defined and can be expressed as follows:

$$d_{i,\,\min} \le d_{i,s} \le d_{i,\,\max}, \quad \forall i \in N_{\mathrm{droop}} \tag{24}$$

The constraints of minimum in-service and out-service time [33]:

$$\begin{aligned} T_{\mathrm{in},m}^{t,s} &\ge T_{\mathrm{in},m}^{\min} \\ T_{\mathrm{out},m}^{t,s} &\ge T_{\mathrm{out},m}^{\min} \end{aligned} \tag{25}$$

The constraints of the ramp up/down rate [33]:

$$\begin{aligned} P_m^{t,s} - P_m^{t-1,s} &\le r_m^{\mathrm{up}} \Delta t \\ P_m^{t-1,s} - P_m^{t,s} &\le r_m^{\mathrm{down}} \Delta t \end{aligned} \tag{26}$$

2.3. EV Scheduling Strategies

When electric vehicles that use the conventional charging method (CCM) get home, they are quickly connected to a charging station. They don't give a hoot about what the system needs. Conventional charging techniques are inefficient because they cause energy loss, decreased system voltage, and congestion. Electric vehicle charging (V2G) and grid-to-vehicle (G2V) power transfers are the main components of the suggested method. Electric vehicle charging and discharging are given priority based on demand. The best way to charge is this specific process. Here, EV drivers put the strain on the system at its lowest possible level. While the load is high, it is not allowed to charge electric vehicles. An effective method that follows the load demand curve charges EVs during low-load hours. A more efficient method of charging results in a more stable voltage profile with less Ptl. Utility companies and electric vehicle owners can now discuss system demand and work together to find more efficient ways to run the system. A system's PADR, or peak-to-average ratio of demand, is a key consideration when making schedules (27). What determines the charge or discharge is the amount of the hourly power ratio (P_{hpr}) (28).

$$PADR = \frac{P_{pd}}{P_{md}} \tag{27}$$

$$P_{hpr} = \frac{P_{hd}}{P_{md}} \tag{28}$$

where P_{md} is an average system demand, P_{pd} is the peak system demand and P_{hd} is a hourly demand.

The following procedures are followed to schedule EVs, utilizing the two quantities mentioned earlier:

(1) The ideal method of charging takes into account the categories of vehicles, the quantity of cars, the rate of charge, and the intervals between trips.

(2) The power ratio (P_{hpr}) and PADR are computed hourly, regardless of whether EVs are taken into account or not.

(3) In order to activate the V2G mode, the power ratio (P_{hpr}) must be less than the average power demand (P_{md}).

(4) If the PR for a given interval time exceeds the overall power demand (P), the car can maintain its state of charge (SoC) by drawing excess power from the grid.

(5) This information will be fed into the WPA approach hourly so that it can calculate the optimal size for renewable DGs.

(6) The process is complete when the EVs reach state of charge and are prepared for the next journey.

3. HYBRID FUZZY-WATERWHEEL PLANT ALGORITHM

When dealing with complicated engineering problems with several restrictions, intelligent optimization strategies are crucial. They outperform conventional algorithms in terms

of efficiency and dependability when it comes to optimizing complicated functions. The ideal location of DGs in reconfigurable MGs can be determined by using a multi-objective optimization algorithm in conjunction with the fuzzy technique, as suggested in this work [39].

3.1. Waterwheel Plant Algorithm (WPA)

In order to optimize the control objectives, the Waterwheel Plant Algorithm (WPA) is suggested. In order to find the optimal solution in its search space, the algorithm employs a group of humans. Moreover, the method is population-based, meaning that it finds the optimal answer via iterations that take into account the collective search capacity of the community. Because the waterwheel can be located anywhere in the search area, the problem variables in the WPA population can take on a wide range of values. The aforementioned allows for the modeling of the initial WPA population stage using an $n \times d$ matrix.:

$$P = \begin{bmatrix} p_{1,1} & \cdots & p_{i,1} & \cdots & p_{1,m} \\ \vdots & \ddots & \vdots & \ddots & \vdots \\ p_{i,1} & \cdots & p_{i,j} & \cdots & p_{i,m} \\ \vdots & \ddots & \vdots & \ddots & \vdots \\ p_{n,1} & \cdots & p_{n,j} & \cdots & p_{n,m} \end{bmatrix} = \begin{bmatrix} p_1 \\ \vdots \\ p_i \\ \vdots \\ p_n \end{bmatrix} \tag{29}$$

$$p_{i,j} = Lb_j + r_{i,j}.\left(Ub_j - Lb_j\right), \quad i = 1, 2, \ldots n, \quad i = 1, 2, \ldots m \tag{30}$$

where P denotes the population matrix, $r_{i,j}$ denotes the random number between [0, 1], Ub_j and Lb_j represents the upper and lower bound of the j-th variable, P_i is the i-th waterwheel, n denotes the number of population, m indicates the number of problem variables, and $p_{i,j}$ denotes the value of j-th variable suggested by i-th waterwheel.

Since every waterwheel in the population solves the optimization problem, the objective function's fitness values are simulated by a vector, as seen in the following example.

$$F = \begin{bmatrix} F_1 \\ \vdots \\ F_i \\ \vdots \\ F_n \end{bmatrix} = \begin{bmatrix} F(X_1) \\ \vdots \\ F(X_i) \\ \vdots \\ F(X_n) \end{bmatrix} \tag{31}$$

Where $F\ (i = 1, 2, \ldots i, \ldots n)$ is the fitness value calculated for the objective function. The next step is to compare all of the fitness values that were acquired. The best value is then used to determine which population member is the best overall. Consequently, the following equation can be used to find the optimal member.

$$B = P_k, \quad f_k = \min(F) \tag{32}$$

Here, B is the obtained best member and P_k is the k-th waterwheel with minimum value of the fitness equal to f_k. Also, the technique includes a two-stage update process for the population members, with the first stage handling exploration and location identification. The second stage involves using the population as a whole to find the optimal solution by convergently improving upon previous ones. Below, we'll go over the mathematical equations for each stage.

Stage 1: The waterwheel typically launches an assault on its target after it has located it; it is a formidable predator. This is how the WPA models mimic the initial stages of the waterwheel's operation, which allows them to update the population process. In mathematical terms, the following equations describe the first stage idea.

$$W = r_1\ .\ (P(t) + 2K) \tag{33}$$

$$P(t+1) = P(t) + W\ .\ (2K + r_2) \tag{34}$$

where r_1 and r_2 denotes the random variables in the range of [0, 2] and [0, 1] respectively. The equation also includes W, a vector that defines the circumference of a circle in which the waterwheel plant would search for prey, and K, an exponential variable that ranges from 0 to 1. If the result stays unchanged after three iterations, the following equation can be used to alter the waterwheel position.

$$P(t+1) = \text{Gaussian}(\mu_P, \sigma) + r_1\left(\frac{P(t) + 2K}{W}\right) \tag{35}$$

IP: 103.207.2.234 On: Tue, 09 Jun 2026 10:13:52
Copyright: American Scientific Publishers
Delivered by Ingenta

Stage 2: Following the process of sucking an insect into a waterwheel, the insect is subsequently moved to a feeding tube. The WPA's second-stage population update makes use of the information obtained from the simulated waterwheel activity of the waterwheel facility. The exploitation power of the algorithm is increased as a result of the fact that it imitates the transport capability to the appropriate tube. In order to quantitatively express this updated position of the waterwheel in relation to the value of the target variable, the following equations are utilized.

$$W = r_3\ .\ (KP_{\text{best}}(t) + r_3\, P(t)) \tag{36}$$

$$P(t+1) = P(t) + KW \tag{37}$$

Where r_3 denotes the random number in the range of [0, 2], $P(t)$ is the current solution at iteration t, and P_{best} is the best solution. The following mutation is implemented in this case as well, in order to prevent being stuck in the local minima.

$$P(t+1) = (r_1 + K) * \sin\left(\frac{F}{C}\theta\right) \tag{38}$$

Where F and C denote the random variables within the range of $[-5, 5]$. Additionally, the K value is updated on the basis of following equation.

$$K = \left(1 + \frac{2 * t^2}{T_{\max}} + F\right) \tag{39}$$

Where T_{max} is the maximum number of iterations. Upon updating all the population members based on 1st and 2nd phase process, a new iteration of algorithm is performed. After then, the new status of the members of the population is computed, and it is updated based on Eqs. (29) to (39) until the final iteration is completed. After the last iteration has been completed, the algorithm will produce the optimal solution that is the best possible fit for the optimization problem that has been presented. An illustration of the WPA's entire execution procedure can be found in Figure 1, which is a flowchart.

3.2. Heuristic Fuzzy

Minimizing P, EmC, and VDF are the three primary goals that are involved in the optimization of the MG. Within the scope of the single-objective optimization issue, the proposed algorithm is capable of providing a satisfactory solution. On the other hand, in order to find a solution to the problem of multi-objective optimization, this work presents the combination of heuristic fuzzy with WPA. Through the utilization of fuzzy logic, distinct membership functions are specified for every objective function, accompanied by upper and lower bands. This provides a greater degree of flexibility when it comes to decision-making. The membership functions that have been generated can also be altered in order to alter the contribution of each objective function of the problem in accordance with the requirements that have been established. A detailed explanation of the objective functions that are involved may be found below.

3.2.1. Power Transmission Loss

The system power transmission loss should be minimized, and to do that, the P (40) and its associated membership function (41) are defined as follows:

$$P = \frac{P_{tl,\text{after}}}{P_{tl,\text{before}}} \tag{40}$$

$$\mu_{PTL} = \begin{cases} 1 & P \le P_{tl,\text{best}} \\ \dfrac{P_{tl,\text{best}} - P}{P_{tl,\text{best}} - P_{tl,\text{worst}}} & P_{tl,\text{worst}} < P < P_{tl,\text{best}} \\ 0 & P \ge P_{tl,\text{worst}} \end{cases} \tag{41}$$

where $P_{tl,\text{after}}$ and $P_{tl,\text{before}}$ refers the power loss after and before attempting reconfiguration, respectively. $P_{tl,\text{best}}$ and $P_{tl,\text{worst}}$ refers previous best configuration reflecting lowest loss and worst configuration loss reflecting highest loss, respectively.

3.2.2. Generation Cost

Power generation should be as cheap as possible. Because of this, the ratio of power generation costs before and after distribution system optimization is defined as follows for a certain demand level (42) and its associated membership function (43):

$$EcC = \frac{TECC_{\text{after}}}{TECC_{\text{before}}} \tag{42}$$

$$\mu_{ECC} = \begin{cases} 1 & EcC \le EcC_{\min} \\ \dfrac{EcC_{\max} - EcC}{EcC_{\max} - EcC_{\min}} & EcC_{\min} < EcC < EcC_{\max} \\ 0 & EcC \ge EcC_{\max} \end{cases} \tag{43}$$

In this work, the upper and lower limits of $EcC_{\min}$ and $EcC_{\max}$ are equal to 0.5 and 1, respectively.

3.2.3. Voltage Deviation Factor

When connected to external equipment, bus voltage limitations are more sensitive power flow constraints. Thus, one goal is to lower generation costs while controlling bus voltage volatility. For each new WPA population, the load flow equation established the system's minimal bus voltage. The membership function (44) determines the difference between the new population's VDF_{after} and the initial VDF_{before}.

$$\mu_{VDF} = \begin{cases} 1.0 & \text{for } VDF_x \le VDF_{\max} \\ \dfrac{VDF_{\max} - VDF_x}{VDF_{\max} - VDF_{\min}} & \text{for } VDF_{\min} < VDF_x < VDF_{\max} \\ 0.0 & \text{for } VDF_x \ge VDF_{\max} \end{cases} \tag{44}$$

IP: 193.25.1.123 On: Tue, 09 Jun 2026 10:13:52
Copyright: American Scientific Publishers
Delivered by Ingenta

$VDF_{\min}$ and $VDF_{\max}$ are considered as 0.05 and 0.1, respectively. VDF_x is expressed as

$$VDF_x = \frac{VDF_{\text{after}}}{VDF_{\text{before}}} \tag{45}$$

$$\mu_D = \min(\mu_{\text{PTL}}\, \mu_{\text{EcC}}, \mu_{\text{VDF}}) \tag{46}$$

The above Eq. (46) is regarded as the fitness function for the WPA, the equation is described here. In light of this, every single population of the WPA generates a solution that is compromised among the three objective functions.

4. SIMULATION RESULTS

4.1. Considered Test Case, Load Pattern, DGs and EVs

For the purpose of validation, the usual RDS for the IEEE 33 bus was taken into consideration under a variety of test situations. 11 kilovolts is the base voltage of the feeder, and the total load that is connected when the feeder is operating at baseload circumstances is. In order to achieve the biggest possible performance advantage, it is necessary to generate two distinct MG-dependent scenarios and determine which type of scenario is more desirable. An illustration of this would be the feeder being split into three and five MGs. A number of different partitioning techniques are used to create the circumstances. After conducting the modeling, it was discovered that each MG

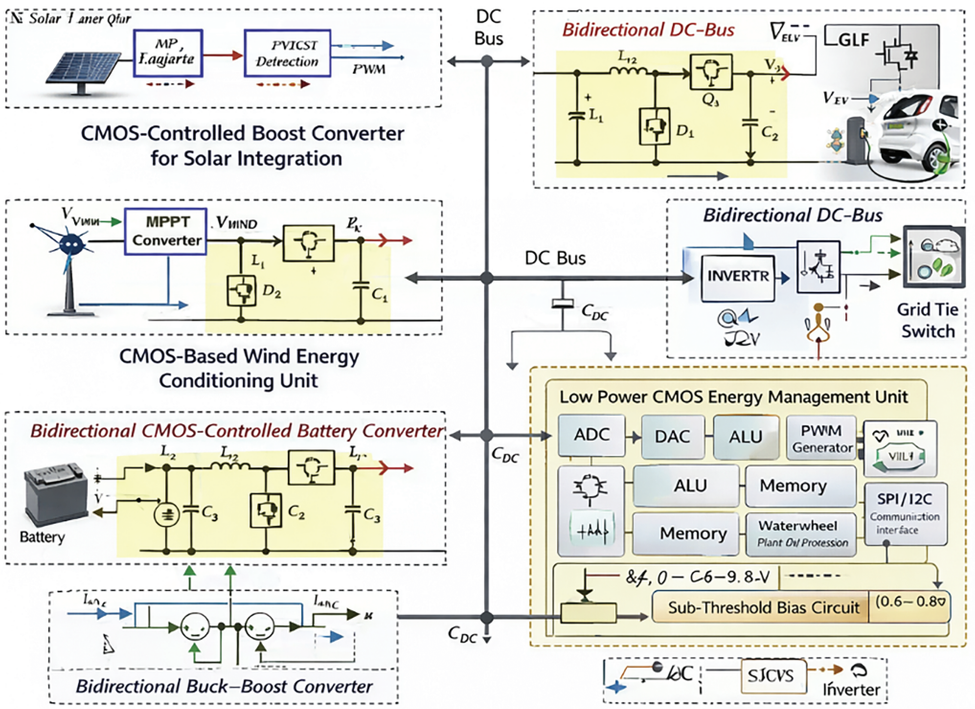


Fig. 2. CMOS-based intelligent microgrid power circuit with bidirectional converters.

IP: 103.207.4.234 On: Tue, 09 Jun 2026 10:13:52
Copyright: American Scientific Publishers
Delivered by Ingenta

received a particular quantity of DG. It ensures that the DG-equipped MGs are able to offer their own support and that there are no load-connected buses that are not met when the baseload condition is present. Because the objective of this proposed work is to determine the ideal configuration of the MGs in conjunction with the presence of the DGs, the initial location of the DGs is determined by the voltage index of the MG. This is done in order to achieve the goal of discovering the optimal configuration. The weak buses of the individual MGs are determined once the base load circumstances have been evaluated. This is done in order to locate the DGs, which are 7, 11, 14, 28, and 17, respectively. The zones of the DGs and load buses that were taken into consideration in the five MGs scenario are depicted in Figure 2. In each of these scenarios, it is presumed that the feeder is capable of supporting a maximum connected load of 4 megawatts, which is greater than the load that is connected to it.

Table I. Characteristic data of PVES, WES.

Parameters	Energy system	
	PVES	WES
Life time	20	12.5
Installation cost ($/kW)	7000	2500
Depreciation time (in years)	20	10
Depreciation cost ($/kW-year)	712.92	372.57
Installed capacity (kW)	100	100

Within the context of the reconfigurable microgrid, the purpose of this study is to investigate the influence of WES and PVES. Table I displays the data that defines the characteristics of the two energy systems that were taken into consideration for the analysis. Figure 3 illustrates the

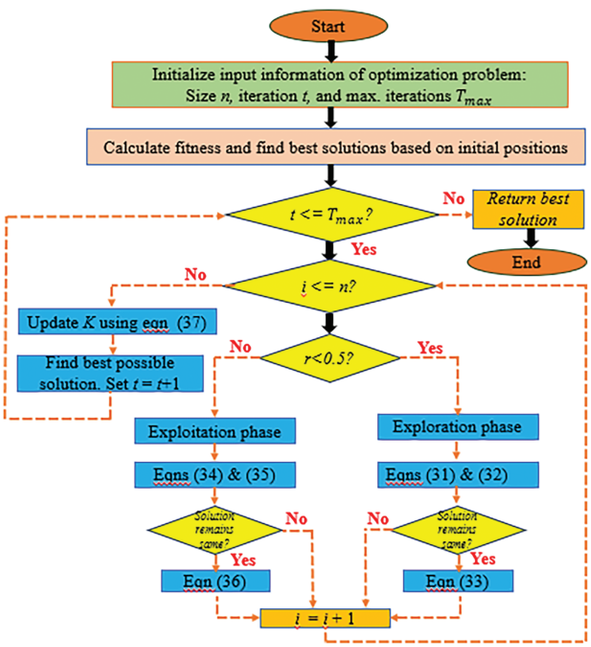


Fig. 3. Flowchart of waterwheel plant algorithm.

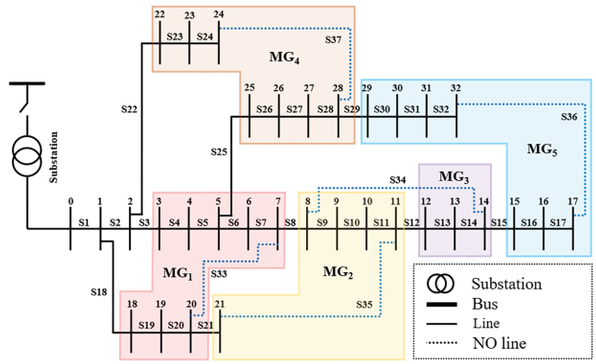


Fig. 4. A single-line diagram of standard IEEE 33-bus RDS modified as 5 MGs.

hour-to-hour efficiency that was taken into consideration for both the WES and the PVES. Specifically, the information that pertains to the energy systems is drawn from [38].

This research also discusses microgrid optimization for electric vehicles. For the MG scenario being analyzed, the 24-hour daily load pattern must be prepared to improve system dynamics. The preparation accounts for hourly power usage swings. Figure 4 shows the MG's estimated power demands per hour of the normal day.

4.2. Implementation of the Strategy

Five active zones were observed because the MG simulated in this work includes five tie-switches. The number of switches in each zone decreases significantly when regarded as reconfiguration solution sets. The iterative system can prevent improbable solution sets. The system switches are grouped by location to increase optimization efficiency and ensure that the iterative process does not miss solution sets that are impossible to execute. Open, closed, permanently closed, and temporarily closed are the four switch classifications [37].

4.2.1. Performance Investigation Only with WES and PVES

This test case was carried out in order to investigate the performance of the microgrid under the conditions of the presence of WES in addition to electric vehicles in the

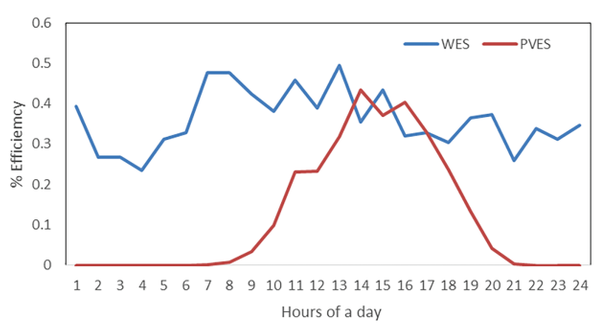


Fig. 5. % efficiency of RES a day.

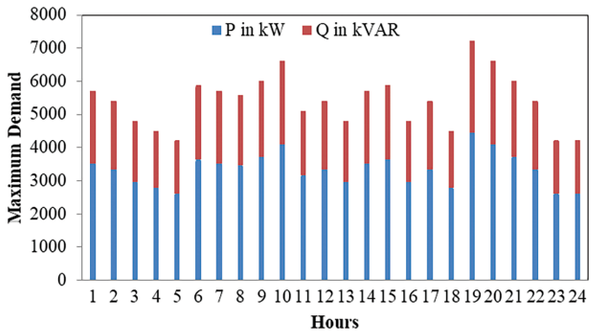


Fig. 6. Demands of a day.

MG. The investigation is carried out under the assumption that the microgrid is only allowed to accommodate five WES. Consequently, the hybrid method that has been suggested maintains five variables for reconfiguration within the microgrid setup. During the execution of the suggested algorithm, fifty iterations and fifty populations are carried out. S7, S9, S14, S32, and S37 are the NOs that have been identified as being the optimal configuration once the execution has been completed successfully. The voltages shown in Figure 5 for the initial configuration bus and those for the final configuration bus when WES is present can be compared. This document details the process of positioning the WES so that it would increase the system bus voltage beyond the initial design. By maintaining bus voltages over 0.95 pu, the system is better able to manage higher bus loading. Branch loading, as shown in Figure 6, guarantees a decrease compared to the original plan. The configuration loss of the system was 202.66 kW, and the transmission loss is now 94.15 kW. The cost of system generation increases to $194.68 per hour due to WES. The results show that WES generation is effective and allows the system to manage higher loads. The WES reduces pollution expenses, first and foremost.

The convergence properties of the algorithm are also compared to those of other algorithms with the same iteration and population parameters. Figure 7 shows that the suggested method converges to the optimal result after 35 iterations faster than the other methods. In the twenty-first

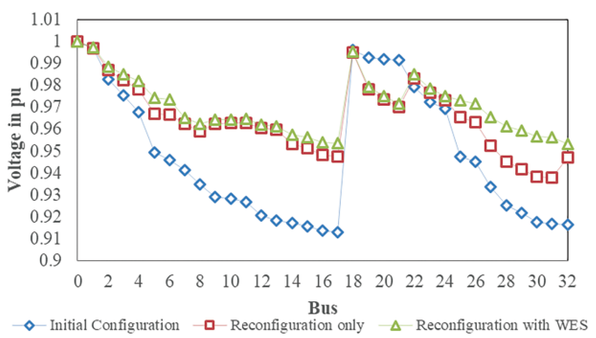


Fig. 7. Comparison of bus voltages with WES.

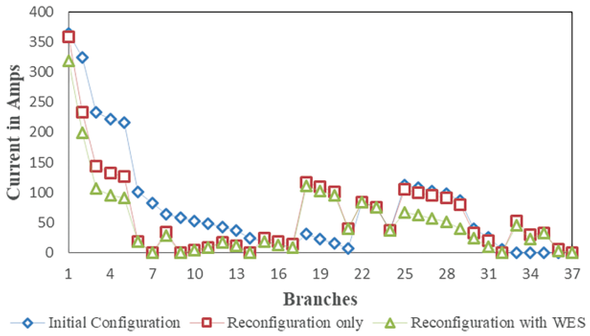


Fig. 8. Comparison of branch currents with WES.

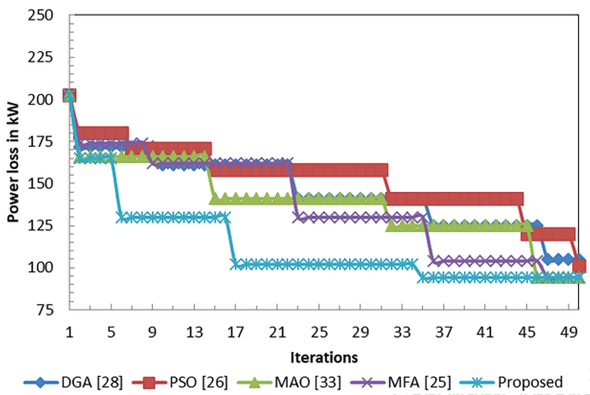


Fig. 9. Convergence characteristic.

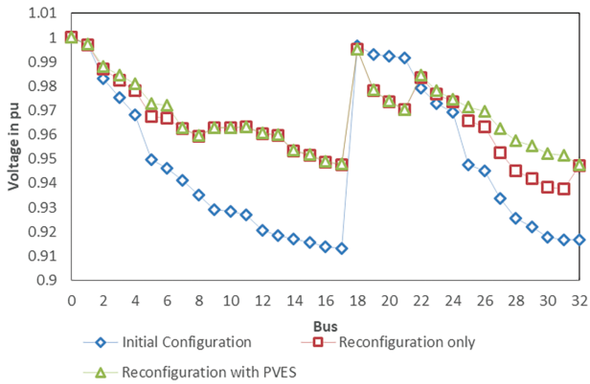


Fig. 10. Comparison of bus voltages with PVES.

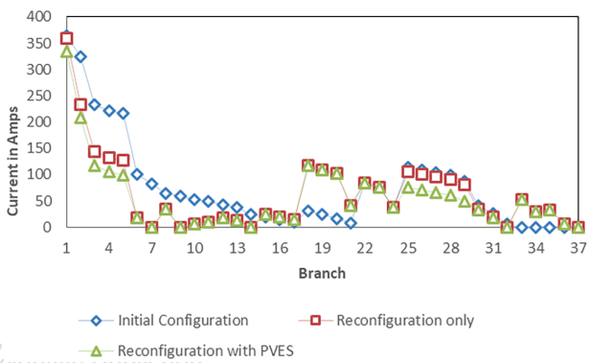


Fig. 11. Comparison of branch currents with PVES.

: Tue,
Copyright: American Scientific Publishers
Delivered by ingenta

iteration, it finds a near-optimal solution. It is not possible for the DGA [28] and PSO [26] algorithms to yield the best result for the given populations and iterations. DGA and PSO determine the optimal solutions after concurrently increasing iterations and populations. Similar to the test case before it, it is assumed that just five PVES are taken into consideration. The optimization process is performed with the assumption that the boundary conditions applied in the previous case also apply to the hybrid approach that is being showcased. The details of the PVES's features are listed in Table I, which is accessible here. After 33 iterations, it has been found that the ideal answer has been reached. As can be observed in Table VI, the ultimate setup outcomes are displayed. Table II presents data on the reduction in power loss that transpired due to the original configuration loss, the ideal configuration, the ideal PVES sites, and the configuration's lowest voltage.

Table II. Optimal solution with PVES under base load condition.

Optimal configuration	Total cost in $/hr	Power loss in kW	Min voltage in pu.
7,9,14,32,37	235.06	108.67	0.9476

The bus voltages and branch currents of the optimal PVES-based microgrid configuration are compared with those of the initial and reconfigured operating conditions (see Figs. 8 and 9). The comparison clearly indicates that the proposed optimization strategy improves the voltage profile and significantly reduces branch current loading, thereby enhancing the overall operational stability and efficiency of the microgrid system.

4.2.2. *Performance Investigation of MG with RES and EVs Under Conventional Charging Method (CCM)*

The operational conditions of the network are continuously deteriorating as a result of the dynamic fluctuations in system demand and the increasing use of electric vehicles. Consequently, the scheduling of electric vehicles needs to be adjusted to accommodate the fluctuating

Table III. Characteristic data of EVs.

Specifications	Ratings
SoC_{min}	0.2
SoC_{max}	0.9
Avg. power consumption/km	0.715 kWh/km
Avg. distance travelled by each EV	30 km

Table IV. Summary of results with WES under daily load pattern.

Hrs.	Total load	Configuration	TGC in $/hr	Loss in kW	Min. voltage in pu
1	3.5293	7,9,14,32,37	187.5549	87.9045	0.9526
2	3.3435	7,9,14,28,32	181.1488	79.5608	0.9560
3	2.9720	9,14,28,33,36	163.9749	60.7445	0.9647
4	2.7863	9,14,28,33,36	156.1776	52.7840	0.9670
5	2.6005	9,14,17,28,33	145.8632	43.1146	0.9718
6	3.6407	7,9,14,32,37	193.4682	93.3470	0.9522
7	3.5293	7,9,14,32,37	184.9260	84.1568	0.9541
8	3.4550	7,9,14,28,32	181.4738	80.4974	0.9575
9	3.7150	7,9,14,32,37	194.6830	94.1552	0.9535
10	4.0865	7,9,14,17,28	213.2629	123.4266	0.9482
11	3.1578	9,14,28,33,36	168.0031	62.5456	0.9642
12	3.3435	7,9,14,28,36	178.2790	75.8388	0.9602
13	2.9720	9,14,28,33,36	158.7290	55.0196	0.9676
14	3.5293	7,9,14,32,37	187.7665	88.2137	0.9525
15	3.6407	7,9,14,32,37	191.0230	89.7753	0.9535
16	2.9720	9,14,28,33,36	162.7243	59.3213	0.9654
17	3.3435	7,9,14,28,32	179.7004	77.6424	0.9577
18	2.7863	9,14,28,33,36	154.5867	51.1264	0.9672
19	4.4580	7,9,14,28,36	230.6737	139.1266	0.9463
20	4.0865	7,9,14,17,28	213.4523	123.7320	0.9482
21	3.7150	7,9,14,32,37	198.5474	99.9832	0.9511
22	3.3435	7,9,14,28,32	179.4905	77.3720	0.9580
23	2.6005	9,14,17,28,33	145.8624	43.0976	0.9720
24	2.6005	9,14,17,28,33	145.0840	42.4053	0.9723

Table VI. Summary of real power loss at the final configuration.

Hrs.	(WES:4, PVES:1)	(WES:3, PVES:2)	(WES:2, PVES:3)	(WES:1, PVES:4)
1	90.4450	93.0794	95.7262	98.3647
2	81.2321	82.9850	84.7318	86.5383
3	62.1899	63.6802	65.1886	66.7549
4	53.9276	55.1014	56.3435	57.6568
5	44.4257	45.8211	47.2326	48.7218
6	95.7087	98.1131	100.5823	103.1584
7	87.3356	90.6370	94.0366	97.4709
8	83.3870	86.4000	89.5586	92.7972
9	96.8975	99.6706	102.5826	105.5833
10	125.6109	127.8717	130.1807	132.5208
11	63.7022	64.8959	66.1525	67.3974
12	76.7658	77.6960	78.6631	79.6365
13	55.8670	56.7357	57.6054	58.4973
14	87.6753	87.1453	86.6156	86.1035
15	90.2002	90.6263	91.0551	91.4870
16	58.8968	58.4769	58.0586	57.6455
17	77.6488	77.6304	77.6244	77.6183
18	51.4278	51.7440	52.0539	52.3654
19	141.0064	142.9366	144.8914	146.8809
20	126.3178	129.0053	131.7361	134.5194
21	101.9069	103.8470	105.8517	107.8988
22	79.4729	81.5796	83.7909	86.0674
23	44.4257	45.8197	47.2326	48.7218
24	43.8336	45.3610	46.9191	48.5554

levels of demand. This research makes use of the Chevrolet Volt EV, which is a well-known electric vehicle currently available on the market. The parameters of the EV are listed in Table III. Each day, sixty electric vehicles (EVs) go to and from work, covering an average distance of thirty kilometers. These EVs leave at eight in the morning and return at five in the afternoon. It is presumed that all electric vehicles must start their journey with a

Table V. Summary of results with PVES under daily load pattern.

Hrs.	Total load in MW	Configuration	TGC in $/hr	Loss in kW	Min. voltage in pu
1	3.5293	7,9,14,28,36	227.3270	101.1755	0.9523
2	3.3435	7,9,14,28,36	218.5910	88.3783	0.9549
3	2.9720	9,14,28,33,36	201.3638	68.3517	0.9613
4	2.7863	9,14,28,33,36	192.7812	59.0420	0.9618
5	2.6005	9,14,17,28,33	184.2233	50.2951	0.9672
6	3.6407	7,9,14,32,37	232.4324	105.7571	0.9474
7	3.5293	7,9,14,28,36	227.2796	101.0982	0.9524
8	3.4550	7,9,14,28,36	223.6625	96.1910	0.9541
9	3.7150	7,9,14,32,37	235.0599	108.6726	0.9476
10	4.0865	7,9,14,28,36	251.1311	134.9264	0.9421
11	3.1578	9,14,28,33,36	204.4917	68.6907	0.9626
12	3.3435	7,9,14,28,32	213.1236	80.6191	0.9567
13	2.9720	9,14,28,33,36	193.9739	59.3993	0.9654
14	3.5293	7,9,14,32,37	217.1146	85.5739	0.9535
15	3.6407	7,9,14,32,37	223.6836	91.9197	0.9528
16	2.9720	9,14,28,33,36	192.0086	57.2335	0.9665
17	3.3435	7,9,14,28,32	210.8573	77.6123	0.9578
18	2.7863	9,14,28,33,36	187.2650	52.6733	0.9672
19	4.4580	7,9,14,28,36	267.3662	148.9057	0.9431
20	4.0865	7,9,14,28,36	252.4961	137.4499	0.9405
21	3.7150	7,9,14,32,37	235.8211	109.9725	0.9474
22	3.3435	7,9,14,28,36	218.5910	88.3783	0.9549
23	2.6005	9,14,17,28,33	184.2233	50.2951	0.9672
24	2.6005	9,14,17,28,33	184.2233	50.2951	0.9672

Table VII. Summary of TGC at the final configuration.

Hrs.	(WES:4, PVES:1)	(WES:3, PVES:2)	(WES:2, PVES:3)	(WES:1, PVES:4)
1	195.5043	203.4579	211.4120	219.3657
2	188.6332	196.1211	203.6088	211.0992
3	171.4493	178.9257	186.4029	193.8827
4	163.4936	170.8109	178.1312	185.4546
5	153.5297	161.1999	168.8709	176.5452
6	201.2557	209.0452	216.8375	224.6345
7	193.3875	201.8544	210.3257	218.7984
8	189.9006	198.3328	206.7714	215.2136
9	202.7513	210.8209	218.8967	226.9764
10	220.8314	228.4034	235.9774	243.5528
11	175.2977	182.5938	189.8928	197.1912
12	185.2467	192.2144	199.1838	206.1535
13	165.7767	172.8254	179.8741	186.9238
14	193.6357	199.5052	205.3747	211.2450
15	197.5550	204.0870	210.6191	217.1513
16	168.5808	174.4376	180.2944	186.1515
17	185.9323	192.1631	198.3945	204.6259
18	161.1220	167.6579	174.1936	180.7294
19	238.0089	245.3462	252.6847	260.0246
20	221.2541	229.0604	236.8686	244.6791
21	205.9989	213.4511	220.9061	228.3630
22	187.3062	195.1221	202.9426	210.7661
23	153.5297	161.1999	168.8709	176.5452
24	152.9052	160.7309	168.5579	176.3883

Delivered by Ingenta

Table VIII. Summary of minimum bus voltage at the final configuration.

Hrs.	(WES:4, PVES:1)	(WES:3, PVES:2)	(WES:2, PVES:3)	(WES:1, PVES:4)
1	0.9526	0.9500	0.9526	0.9500
2	0.9560	0.9567	0.9567	0.9567
3	0.9645	0.9631	0.9629	0.9625
4	0.9660	0.9659	0.9645	0.9632
5	0.9708	0.9699	0.9697	0.9685
6	0.9522	0.9498	0.9498	0.9498
7	0.9541	0.9509	0.9508	0.9508
8	0.9577	0.9542	0.9541	0.9546
9	0.9507	0.9510	0.9504	0.9484
10	0.9482	0.9482	0.9446	0.9440
11	0.9644	0.9643	0.9629	0.9629
12	0.9584	0.9573	0.9573	0.9562
13	0.9674	0.9665	0.9665	0.9661
14	0.9531	0.9530	0.9535	0.9530
15	0.9535	0.9531	0.9531	0.9528
16	0.9659	0.9659	0.9660	0.9664
17	0.9576	0.9578	0.9578	0.9578
18	0.9672	0.9670	0.9680	0.9676
19	0.9448	0.9447	0.9438	0.9431
20	0.9482	0.9481	0.9445	0.9428
21	0.9493	0.9493	0.9492	0.9475
22	0.9557	0.9557	0.9572	0.9571
23	0.9708	0.9698	0.9697	0.9685
24	0.9713	0.9701	0.9700	0.9686

IP: 103.207.4.234 On: Tue, 19 Jan 2021 ... Copyright: American Scientific Publishers ... Delivered by Ingenta

full charge, and there is no means to replenish the battery outside of the hours when the vehicle is in motion. In addition, electric vehicles require a considerable amount of time to charge their batteries, which is contingent upon the distance traveled or being supplied to the grid. Additionally, it has been contemplated that electric vehicles (EVs) and the power grid might be connected through a communication system that operates in both directions. Through the use of this channel, information may be transmitted between them, which enables combined scheduling of DG and EV. Furthermore, as a consequence of this, data is sent from one channel to the next without any delay. When it comes to the CCM, the optimal locations for charging electric vehicles are the 12, 18, 21, 22, and 29 nodes. Individual MGs identify these nodes as powerful busses. Maintaining MG operation during changing demand proves the hybrid algorithm's efficacy. The scientific investigation uses Figure 11′s usual load pattern and Figure 10′s typical WES hourly variable efficiency. The ideal solution is determined after implementing the algorithm under hourly changing generation and load patterns, shown in Table IV, the NO's for the optimal structure as S_7, S_9, S_{14}, S_{32}, and S_{37}.

The process of optimization has been carried out by taking into account the daily efficiency features of PVES and the daily load pattern, which are depicted in Figures 10 and 11, respectively. This table provides a summary of the results that were obtained under different load circumstances. According to Table V, it has been determined that the NOs for the best structure are S7, S9, S14, S32, and S37 in the majority of the solutions that have been taken into consideration. It is advised that the PVES be connected at the sites that have been determined in order to achieve optimal solutions under a variety of scenarios. During the execution of this test case, the only thing that is taken into consideration is the presence of PVES in the microgrid.

4.2.3. *Performance Investigation of MG with the Presence of WES and PVES, Optimized Charging Method (OCM)*

According to this test case, the various combinations of WES and PVES are explored by constraining a total of five numbers of ES for the purpose of power generation. The OCM technology allows for the calculation of the right amount of time to charge electric vehicles by taking into consideration the power demand of the system. The 12, 18, 21, 22, and 29 buses are the best places for electric vehicles to be situated in an OCM. The study considers WES and PVES equivalent efficiency each hour under various load needs throughout the day. The evaluation and OCM analysis are done together. This system lets electric cars charge and share electricity with the grid. OCM calculates the best time to charge electric vehicles based on system load demand. A population size of fifty and a maximum iteration of one hundred were maintained during optimization using the suggested approach.

The suggested hybrid algorithm finds the optimum solution for every combination that meets certain characteristic requirements. Optimal results are obtained under various load conditions for WES, PVES, and battery electric cars. The microgrid's genuine power loss, producing cost, and minimum bus voltage are shown in Tables VI–VIII.

During the course of the experiments, the following observations were made:

(i) In many RES combinations, the optimum settings are essentially identical across all scenarios throughout the day.

(ii) The optimal sites for ES, whether WES or PVES, are almost comparable.

(iii) When the number of WES in the system increases, both the total generating cost and real power loss decrease. Due to WES' lower generation cost than PVES.

(iv) PVES does not generate power for 12 hours but has an efficiency of over 25% for 8 hours. However, PVES would be more efficient than WES in summer. WES daily efficiencies are higher than PVES.

(v) When RDGs and EVCS are allocated simultaneously, the voltage profile improves and RES uncertainty in DS decreases compared to a single allocation method.

5. CONCLUSION

In this article, a method is proposed for locating and determining the size of charging stations for electric vehi-

cles (EVs) and renewable energy generators (RDGs). The proposed method was carried out on a IEEE 33 RDS. Although it requires fewer iterations, the proposed method is superior to other approaches. When compared to a single allocation system, the use of EVCS and RDGs simultaneously resulted in an improvement in the voltage profile and a reduction in the uncertainty associated with renewable energy sources. CCM can be seen in two different forms: G2V + V2G and OCM, which reduces the amount of PLoss. Through the use of WES, PVES, and both, this study investigated the performance of microgrids. In every scenario (G2V and V2G), the MG is responsible for validating the EV features. For the purpose of analyzing load dispatch in the context of hour-to-hour daily pattern variations, the 24-hour characteristics of ES were utilized. The results of the simulation demonstrate that the proposed method offers the best possible answer, and the structure that has been optimized is unquestionably superior to the one that is already in place. It is the goal of the strategy that has been disclosed to minimize power loss and enhance voltage profile while simultaneously improving RDG allocation and DS electric vehicle scheduling.

6. DECLARATION

Conflicts of Interest

The authors declare no conflicts of interest.

IP: 103.207.4.234 On: Tue, 09 Dec 2025 10:13:52
Copyright: American Scientific Publishers
Delivered by Ingenta

References and Notes

1. Singh, M., Khadkikar, V., Chandra, A. and Varma, R.K., **2011**. Grid interconnection of renewable energy sources at the distribution level with power-quality improvement features. *IEEE Transactions on Power Delivery*, *26*(1), pp.307–315.
2. Kavousi-Fard, A., Khodaei, A. and Bahramirad, S., **2016**. Improved efficiency, enhanced reliability and reduced cost: The transition from static microgrids to reconfigurable microgrids. *The Electricity Journal*, *29*(10), pp.22–27.
3. Parhizi, S., Lotfi, H., Khodaei, A. and Bahramirad, S., **2015**. State of the Art in research on microgrids: A review. *IEEE Access*, *3*, pp.890–925.
4. Roy, N.K., Pota, H.R. and Anwar, A., **2012**. A New Approach for Wind and Solar Type DG Placement in Power Distribution Networks to Enhance Systems Stability, *2012 IEEE International Power Engineering and Optimization Conference Melaka*, Malaysia, Melaka, Malaysia, pp.296–301, DOI: 10.1109/PEOCO.2012.6230878.
5. Kayal, P. and Chanda, C.K., **2013**. Placement of wind and solar based DGs in distribution system for power loss minimization and voltage stability improvement. *International Journal of Electrical Power & Energy Systems*, *53*, pp.795–809.
6. Baran, M., Wu, F., Dugan, R. and McDermott, T., **2019**. Impact of distributed generation on protection and voltage regulation of distribution systems: A review. *Renewable and Sustainable Energy Reviews*, *105*, pp.157–167.
7. Acharya, N., Mahat, P. and Mithulananthan, N., **2022**. Optimal allocation of distributed generation and capacitor banks using probabilistic generation models with correlations. *Applied Energy*, *307*, pp.112–120.
8. Tan, W.-S., Hassan, M.Y., Majid, M.S. and Abdul Rahman, H., **2013**. Optimal distributed renewable generation planning: A review of different approaches. *Renewable and Sustainable Energy Reviews*, *18*, pp.626–645.
9. Sultana, B., Mustafa, M.W., Sultana, U. and Bhatti, A.R., **2016**. Review on reliability improvement and power loss reduction in distribution system via network reconfiguration. *Renewable and Sustainable Energy Reviews*, *66*, pp.297–310.
10. Teshome, D.F. and Lian, K.L., **2018**. Comprehensive mixed-integer linear programming model for distribution system reconfiguration considering DGs. *IET Generation, Transmission & Distribution*, *12*(20), pp.4515–4523.
11. Yang, K., Michael, Li, R., Wang, J. and Bäck, T., **2014**. Power distribution network reconfiguration by evolutionary integer programming. *Lecture Notes in Computer Science*, pp.11–23.
12. Jazebi, S., Moghimi Hadji, M. and Naghizadeh, R.A., **2014**. Distribution network reconfiguration in the presence of harmonic loads: Optimization techniques and analysis. *IEEE Transactions on Smart Grid*, *5*(4), pp.1929–1937.
13. Ghaweta, A.B. and Liao, Y., **2019**. Optimal distribution feeder reconfiguration with optimal planning of distributed generation for loss reduction and voltage improvement using differential evolution algorithm. *International Journal of Forensic Software Engineering*, *1*(1), pp.245–252.
14. Ganguly, S. and Samajpati, D., **2015**. Distributed generation allocation on radial distribution networks under uncertainties of load and generation using genetic algorithm. *IEEE Transactions on Sustainable Energy*, *6*(3), pp.688–697.
15. Radosavljević, J., Arsić, N., Milovanović, M. and Ktena, A., **2020**. Optimal placement and sizing of renewable distributed generation using hybrid metaheuristic algorithm. *Journal of Modern Power Systems and Clean Energy*, *8*(3), pp.499–510.
16. Gazijahani, F.S. and Salehi, J., **2017**. Stochastic multi-objective framework for optimal dynamic planning of interconnected microgrids. *IET Renewable Power Generation*, *11*(14), pp.1749–1759.
17. Wang, Z., Chen, B., Wang, J., Kim, J. and Begovic, M.M., **2014**. Robust optimization based optimal DG placement in microgrids. *IEEE Transactions on Smart Grid*, *5*(5), pp.2173–2182.
18. Hemeida, M.G., Alkhalaf, S., Senjyu, T., Ibrahim, A., Ahmed, M. and Bahaa-Eldin, A.M., **2021**. Optimal probabilistic location of DGs using monte Carlo simulation based different bio-inspired algorithms. *Ain Shams Engineering Journal*, *12*(3), pp.2735–2762.
19. Khorram-Nia, R., Bahmani-Firouzi, B. and Simab, M., **2018**. Optimal switching in reconfigurable microgrids considering electric vehicles and renewable energy sources. *Journal of Renewable and Sustainable Energy*, *10*(4), pp.88–96.
20. Nguyen, T.T. and Truong, A.V., **2015**. Distribution network reconfiguration for power loss minimization and voltage profile improvement using cuckoo search algorithm. *International Journal of Electrical Power & Energy Systems*, *68*, pp.233–242, DOI: 10.1016/j.ijepes.2014.12.075.
21. Peng, X., Lin, L., Zheng, W. and Liu, Y., **2015**. Crisscross optimization algorithm and monte Carlo simulation for solving optimal distributed generation allocation problem. *Energies*, *8*(12), pp.13641–13659.
22. Sedighizadeh, M., Esmaili, M. and Esmaeili, M., **2014**. Application of the hybrid Big bang-big crunch algorithm to optimal reconfiguration and distributed generation power allocation in distribution systems. *Energy (Oxf)*, *76*, pp.920–930.
23. Alanazi, M.S., **2022**. A MILP model for optimal renewable wind DG allocation in smart distribution systems considering voltage stability and line loss. *Alexandria Engineering Journal*, *61*(8), pp.5887–5901.
24. Zhou, Z., Zhang, J., Liu, P., Li, Z., Georgiadis, M.C. and Pistikopoulos, E.N., **2013**. A two-stage stochastic programming

model for the optimal design of distributed energy systems. *Applied Energy*, *103*, pp.135–144.

25. Kumar, A., Rajasekar, S., Prakash, M., Srinivasan, R. and Balachander, K., **2021**. Research progress on optimal sizing and energy management strategy of wind-solar-hydrogen hybrid energy systems. *Distributed Energy Resources*, *6*(4), pp.1–14.

26. Merzoug, Y., Abdelkrim, B. and Larbi, B., **2020**. Distribution network reconfiguration for loss reduction using PSO method. *International Journal of Electrical and Computer Engineering*, *10*(5), pp.301–309.

27. Abdelsalam, A.A., **2020**. Optimal distributed energy resources allocation for enriching reliability and economic benefits using sine-cosine algorithm. *Technology and Economics of Smart Grids and Sustainable Energy. Springer Science and Business Media LLC*, *5*(1), pp.411–420.

28. Ali, Z.M., Al-Dhaifallah, M. and Komikawa, T., **2022**. Optimal operation and scheduling of a multi-generation microgrid using grasshopper optimization algorithm with cost reduction. *Soft Computing*, *26*(18), pp.9369–9384.

29. Morshidi, M., Nurulhady, I., Musirin, S.R.A., Rahim, M. and Rafi Adzman, M.H., **2018**. Whale optimization algorithm based technique for distributed generation installation in distribution system. *Bulletin of Electrical Engineering and Informatics*, *7*(3), pp.442–449.

30. El-Ela, A.A.A., El-Sehiemy, R.A. and Abbas, A.S., **2018**. Optimal placement and sizing of distributed generation and capacitor banks in distribution systems using water cycle algorithm. *IEEE Systems Journal. Institute of Electrical and Electronics Engineers (IEEE)*, *12*(4), pp.3629–3636.

31. Wang, X., Srinivasan, T., Kim, H. and Ra, I.-H., **2020**. Exploration of DG placement strategy of microgrids via FMFO algorithm: Considering increasing power demand and diverse DG combinations. *Energies*, *13*(24), pp.155–163.

32. Kennedy, J., Eberhart, R., Sivanandam, P. and Baskar, S., **2021**. ABC algorithm based optimal sizing and placement of DGs in distribution networks considering multiple objectives. *Ain Shams Engineering Journal*, *12*(1), pp.697–708.

33. Mahdavi, M., Schmitt, K.E.K. and Jurado, F., **2023**. Robust distribution network reconfiguration in the presence of distributed generation under uncertainty in demand and load variations. *IEEE Transactions on Power Delivery*, *38*(5), pp.3480–3495.

34. Wibowo, R. and Seto, O., **2022**. Optimal placement of intermittent DG renewable energy and capacitor bank for power losses reduction and voltage profile improvement in microgrids systems. *Journal of Engineering Science and Technology*, *17*(5), pp.3539–3554.

35. Wu, H., Dong, P. and Liu, M., **2020**. Distribution network reconfiguration for loss reduction and voltage stability with random fuzzy uncertainties of renewable energy generation and load. *IEEE Transactions Industrial Information*, *16*(9), pp.5655–5666.

36. Ramadan, A., Ebeed, M., Kamel, S., Abdelaziz, A.Y. and Haes Alhelou, H., **2021**. Scenario-based stochastic framework for optimal planning of distribution systems including renewable-based DG units. *Sustainability*, *13*(6), pp.521–530.

37. Srinivasan, T., Wang, X., Kim, H.J. and Ra, I.-H., **2020**. Performance enhancement for microgrids under the demand uncertainties with the presence of multiple DGs through stochastic ranking algorithm. *Journal of Electrical Engineering & Technology*, *16*(1), pp.223–238.

38. Ali, Z.M., Diaaeldin, I.M., Abdel Aleem, S.H.E., El-Rafei, A., Abdelaziz, A.Y. and Jurado, F., **2020**. Scenario-based network reconfiguration and renewable energy resources integration in large-scale distribution systems considering parameters uncertainty. *Mathematics*, *9*(1), pp.640–648.

39. Mina, W.A., **2021**. Performance enhancement of distribution systems via distribution network reconfiguration and distributed generator allocation considering uncertain environment. *Journal of Modern Power Systems and Clean Energy*, *10*(3), pp.647–655.

40. Hemeida, M.G., Alkhalaf, S., Senjyu, T., Ibrahim, A., Ahmed, M. and Bahaa-Eldin, A.M., **2021**. Optimal probabilistic location of DGs using monte Carlo simulation based different bio-inspired algorithms. *Ain Shams Engineering Journal*, *12*(3), pp.2735–2762.

41. Mansouri, N., Lashab, A., Guerrero, J.M. and Cherif, A., **2020**. Photovoltaic power plants in electrical distribution networks: A review on their impact and solutions. *IET Renewable Power Generation*, *14*(12), pp.2114–2125.

IP: 103.47.132.23 On: Tue, 09 Dec 2025 13:13:52
Copyright: American Scientific Publishers
Delivered by Ingenta